J|A|C|S
ARTICLES
Published on Web 06/20/2006

Quantum Interference as the Source of Steric Asymmetry and Parity Propensity Rules in NO−Rare Gas Inelastic Scattering

Arjan Gijsbertsen,[†] Harold Linnartz,[‡] Craig A. Taatjes,[§] and Steven Stolte*[,†,⊥]

Contribution from the Laser Centre and Department of Physical Chemistry, Vrije Universiteit Amsterdam, De Boelelaan 1083, 1081 HV Amsterdam, The Netherlands, Sackler Laboratory for Astrophysics, Leiden Observatory, P.O. Box 9513, 2300 RA Leiden, The Netherlands, Combustion Research Facility, Mailstop 9055, Sandia National Laboratories, Livermore, California 94550, and Unidad de Láseres y Haces Moleculares, Instituto Pluridisciplinar, Universidad Complutense de Madrid, C/ Juan XXIII-1°, 28040-Madrid, Spain

Received December 5, 2005; E-mail: stolte@few.vu.nl

Abstract: Rotationally inelastic scattering of rare gas atoms and oriented NO molecules exhibits a remarkable alternation in the sign of steric asymmetry between even and odd changes in rotational quantum number. This effect has also been found in full quantum-mechanical scattering calculations. However, until now no physical picture has been given for the alternation. In this work, a newly developed quasi-quantum treatment (QQT) provides the first demonstration that quantum interferences between different orientations of the repulsive potential (that are present in the oriented wave function) are the source of this alternation. Further, from application of the treatment to collisions of nonoriented molecules, a previously unrecognized propensity rule is derived. The angular dependence of the cross sections for excitation to neighboring rotational states with the same parity is shown to be similar, except for a prefactor. Experimental results are presented to support this rule. Unlike conventional quantum-mechanical (or semiclassical) treatments, QQT requires no summation over the orbital angular momentum quantum number *l* or integration over the impact parameter *b*. This eliminates the need to solve large sets of coupled differential equations that couple *l* and rotational state channels among which interference can occur. The QQT provides a physical interpretation of the scattering amplitude that can be represented by a Legendre moment. Application of the QQT on a simple hard-shell potential leads to near-quantitative agreement with experimental observations.

1. Introduction

Inelastic scattering of open-shell molecules provides detailed information on collision-induced energy transfer, necessary for understanding fundamental processes in chemical reactions.[1,2] It has been a long-standing goal in molecular sciences to steer chemical reactions, and for this it is a prerequisite to understand and predict the outcome of a reactive encounter. One way to achieve this goal is to exploit nature's preference for directionality and to control (steer) a reaction by orienting molecules before they collide and eventually react.

Measurements of rotationally inelastic scattering of rare gases with oriented NO molecules — i.e., N-end or O-end collisions — have shown a large dependence on the initial orientation.[3−8] This dependence can be expressed by the molecular steric asymmetry ratio (*S*):

$$S_{i\rightarrow f} = \frac{\sigma_{R-NO} - \sigma_{R-ON}}{\sigma_{R-NO} + \sigma_{R-ON}} \quad (1)$$

in which σ_{R-NO} and σ_{R-ON} denote the cross sections for rotational energy transfer from the initial (i) state to the final (f) state when the rare gas atom R impinges onto the N-end or the O-end, respectively.

In experiments described in refs 3−6, a hexapole has been used to state-select NO in the upper component ($\epsilon = -1$) of the Λ-doublet of the $^2\Pi_{1/2}$ rotational ground state ($j = {}^1/_2$), where ϵ is the symmetry index ($\epsilon = -1, 1$) and *j* the rotational angular momentum quantum number. The NO molecules are subsequently oriented in a homogeneous electrostatic field. When a beam of Ar or He crosses the beam of oriented NO, collisions induce rotational excitation of the NO molecules from the rovibrational ground state to higher rotational levels ($j = {}^1/_2$, $\bar{\Omega}$

[†] Vrije Universiteit Amsterdam.
[‡] Leiden Observatory.
[§] Sandia National Laboratories.
[⊥] Universidad Complutense de Madrid.

(1) Kohguchi, H.; Suzuki, T.; Alexander, M. H. *Science* **2001**, *294*, 832.
(2) Levine, R. D. *Reaction Dynamics*; Cambridge University Press: Cambridge, UK, 2005.
(3) van Leuken, J. L.; Bulthuis, J.; Stolte, S.; Snijders, J. G. *Chem. Phys. Lett.* **1996**, *260*, 595.
(4) de Lange, M. J. L.; Drabbels, M.; Griffiths, P. T.; Bulthuis, J.; Snijders, J. G. *Chem. Phys. Lett.* **1999**, *313*, 491.
(5) de Lange, M. J. L. Steric and State-to-State Dependence of Rotationally Inelastic Scattering of NO. Ph.D. Thesis, Vrije Universiteit Amsterdam, 2003.
(6) de Lange, M. J. L.; Stolte, S.; Taatjes, C. A.; Kłos, J.; Groenenboom, G. C.; Avoird, A. v. d. *J. Chem. Phys.* **2004**, *121*, 11691.
(7) Gijsbertsen, A.; de Lange, M. J. L.; Wiskerke, A. E.; Linnartz, H.; Drabbels, M.; Klos, J.; Stolte, S. *Chem. Phys.* **2004**, *301*, 293.
(8) Alexander, M. H.; Stolte, S. *J. Chem. Phys.* **2000**, *112*, 8017.

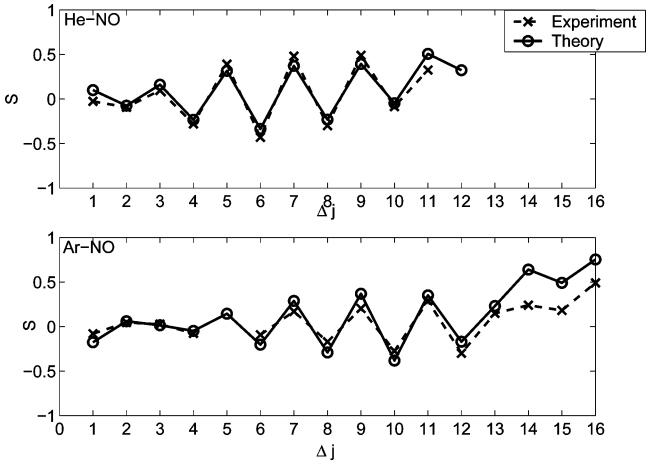

Figure 1. Dependence of the observed and theoretical steric asymmetry ratios on the rotational excitation $\Delta j = j' - j$ with $\bar{\Omega}' = {}^1/_2$, $\epsilon' = -1$, plotted for He colliding with NO at $E_{tr} = 514$ cm^{-1} (top)[6] and for Ar with No at $E_{tr} = 475$ cm^{-1} (bottom).[5] If collisions onto the N-end have a larger cross section for excitation to a certain rotational state, S is positive, and vice versa. The experimental steric asymmetry SA has been multiplied by -1 to match the plotted theoretical result $S_{i\rightarrow f}$.[6] There still is an unresolved sign discrepancy between theory and experiment, as discussed in detail in refs 7 and 11.

$= {}^1/_2, \epsilon \rightarrow j', \bar{\Omega}', \epsilon'$). Ω is the projection of the electronic angular momentum on the molecular axis, and $\bar{\Omega}$ is the absolute value of this projection. Laser-induced fluorescence (LIF) was used to measure the ratio of inelastic collision cross sections in the two orientations in these experiments.[3,4,6]

Until now, no clear physical explanation could be given for the observed dependence of $S_{i\rightarrow f}$ on the final rotational state of the NO molecule: collisions with an odd change in rotational quantum number $\Delta j = j' - j$ have a strong preference for the N-end, whereas final rotational states with even Δj result mostly from O-end collisions. A full quantum treatment (using HIBRIDON[6,8,9]) yields a fair agreement with the observed orientation dependence of the integral cross section but provides no understanding of the undulatory dependence of S on Δj.[10] In conventional scattering calculations, the desired cross sections are obtained from multiple summations over products of **T**-matrix elements and provide no intuitive picture of the underlying collision propensity. Theoretical exact close-coupling (CC) calculations and experimental results are presented in Figure 1 to illustrate the dependence of S on Δj.

Alexander and Stolte[8] showed that the undulatory behavior of S is insensitive to the angular dependence of the long-range part of the Ar−NO potential. Its most prominent features are governed by the anisotropy of the repulsive part of the potential, to which S is very sensitive. However, Alexander and Stolte[8] did not succeed in establishing an explanation for the observed alternation of $S_{i\rightarrow f}$ as a function of $\Delta j = j' - j$, nor to provide a clear link between this behavior and the shape of the anisotropic potential. In this paper we will explain the observed steric effects by introducing a quasi-quantum treatment (QQT) of the collision problem. The alternation between N-end and O-end preference is demonstrated in this work to correspond to a quantum interference phenomenon between scattering events from different molecular orientations.

The conventional exact CC solution of the scattering problem of a rare gas atom R and a heteronuclear rigid diatomic (NO) requires the expansion of the incoming plane wave e^{ikZ} into an infinite sum of Legendre polynomials $P_l(\cos\theta)$, where θ is the scattering angle. Each $P_l(\cos\theta)$ is multiplied by an incoming and outgoing spherical wave $e^{\pm i(kR - l\pi/2)}/(kR)$ to yield the proper plane wave. The absolute value of the position vector is written as R and the orbital quantum number as l. The incoming wavenumber k is given by

$$k \equiv \frac{1}{\hbar}\sqrt{\frac{2E_{tr}}{(m_{NO} + m_R)/(m_{NO}m_R)}} \tag{2}$$

The semiclassical impact parameter b (see Figure 2) is related to the orbital angular momentum quantum number l as

$$b \approx \frac{l + {}^1/_2}{k} \tag{3}$$

The quantum number l couples with the NO rotational quantum number j to yield the total angular momentum quantum number J. Both J and the overall parity of the total wave function are conserved by the scattering Hamiltonian. To solve the He−NO inelastic scattering problem at $E_{tr} \approx 500$ cm^{-1}, the maximum value of J becomes as large as 120.5.[12,13] At each value of J, one has to solve a large set of coupled differential equations that contain all relevant scattering channels j, l, $\bar{\Omega}$, and ϵ that influence the outcome of the scattering process. In the example of He−NO, the number of coupled differential equations that need to be solved numerically is typically as large as 1300 at a single value of J and parity.[12] State-of-the-art computational possibilities still exclude exact calculations on molecule−molecule scattering, for which there are many more channels. An exception is the case of low collision energies or large splitting between the rotational states (H_2-like molecules). Conventional quantum treatments provide good qualitative results, but these elaborate numerical methods yield little insight into the actual physics behind phenomena and their behavior under different circumstances. Calculation times are often too long to adjust the input parameters and learn the behavior of the system as a function of these parameters. To overcome theoretical limitations, a large number of approximative methods to solve inelastic scattering problems have been developed since the 1960s.[14] Among these, the semiclassical version of the infinite order sudden (IOS) approximation has turned out to be particularly useful, as it facilitates rapid calculation.[15−18]

Generally speaking, there are two types of sudden approximation. In the first one, the molecular axis is assumed to remain fixed in space, and the scattering paths are fully determined by the isotropic part of the potential. A rotational transition probability is treated as a time-dependent perturbation resulting from the anisotropic part of the potential. The

(9) Alexander, M. H.; et al. HIBRIDON (http://www.chem.umd.edu/physical/alexander/hibridon/).
(10) Alexander, M. H. *Faraday Discuss. Chem. Soc.* **1999**, *113*, 437−454.
(11) Gijsbertsen, A.; Linnartz, H.; Klos, J.; Stolte, S. *Phys. Scr.* **2005**, *72*, 1−5.
(12) Groenenboom, G. C., private communications, 2005.
(13) Gijsbertsen, A.; Linnartz, H.; Rus, G.; Wiskerke, A. E.; Stolte, S.; Chandler, D. W.; Klos, J. *J. Chem. Phys.* **2005**, *123*, 224305.
(14) Arthurs, A. M.; Dalgarno, A. *Proc. R. Soc. (London), Ser. A* **1960**, *256*, 540.
(15) Schinke, R.; Bowman, J. M. *Rotational Rainbows in Atom−Diatom Scattering*; Springer-Verlag: Berlin, 1983; p 61.
(16) Buck, U.; Khare, V. *J. Chem. Phys.* **1977**, *97*, 215.
(17) Dickenson, A. S.; Richards, D. *Adv. At. Mol. Phys.* **1982**, *18*, 165.
(18) Korsch, H. J.; Ernesti, A. *J. Phys. B* **1992**, *25*, 3565.

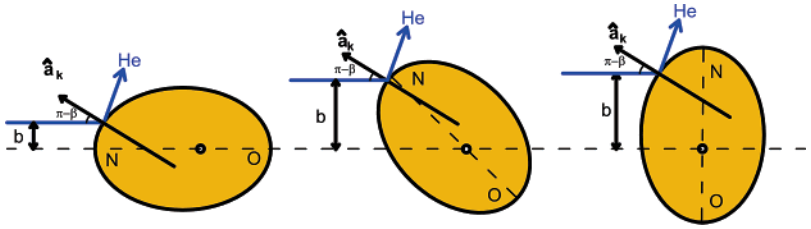

Figure 2. All orientations are present in the oriented wave function. Constructive and destructive interference between these waves will occur, dependent on the difference in path length. The potential can cause scattering under a certain angle for many different impact parameters. Note that for a hard shell as drawn here, the kinematic apse $\hat{\boldsymbol{a}}$ coincides with the surface normal $\hat{\boldsymbol{n}}$.

exponential form of the **S**-matrix is not approximated, but the resulting phase shifts are from a first-order approximation of the anisotropy of the potential. The angle between the specified molecular axis and the position vector $\boldsymbol{R}$ between the centers of mass of the atom and molecule is the main collision variable.[19−21]

Following Curtiss,[22] Pack[23] and McGuire and Kouri[24] described collisions of atoms and diatomics in terms of body fixed or rotating coordinate frames. In this second type of sudden approximation, the molecular axis $\boldsymbol{r}$ is assumed to be fixed in respect to $\boldsymbol{R}$ and not in space ($\hat{\boldsymbol{R}}\cdot\hat{\boldsymbol{r}} \equiv \cos\gamma_R$). The centrifugal term in the Schrödinger equation is simplified by approximating $\bar{l} = l$ and $l' = \bar{l}$ (with l and l' the initial and final orbital angular momentum), which drastically reduces the number of coupled equations. This decoupling of the centrifugal barrier is also referred to as the "centrifugal sudden approximation". It leads to a phase shift calculation that is of infinite order in the anisotropy of the potential for each orientation angle γ of the molecule. When the energy of the rotational states is taken into account, one refers to this method as the "coupled states" (CS) approximation. When this energy is ignored, one speaks about the "infinite order sudden" (IOS) approximation.

Today, the IOS approximation is often applied when one is prevented from carrying out numerically demanding close-coupling calculations for practical reasons. The IOS and CS approximations usually yield satisfactory results in the calculation of m, m' degeneracy-averaged collision cross sections, but they are well known to err in predicting the m, m' or steric dependence of the inelastic collision cross section (m and m' are the projections of the total angular momentum $\boldsymbol{j}$ on a space-fixed axis). This shortcoming can be alleviated by assuming a hard-shell-like "point contact interaction" (PCI) at the turning point.[25,26] Khare, Kouri, and Hoffman[27,28] subsequently showed explicitly that there is a propensity for preserving j_z when using an apse (geometric or kinematic) as a quantization axis. The two apses coincide for elastic collisions and point about parallel to $\boldsymbol{R}$ at the turning point in the case of a near-isotropic (near-spherical) potential. The kinematic apse (KA) direction is that along which momentum is transferred in the hard-shell approximation. In general, the kinematic apse is Δj dependent while the geometric apse is not. It was shown that one can obtain reasonable differential cross sections quantized in the space-fixed frame by calculating and transforming only the $\Delta m = 0$ scattering amplitude from the KA frame for a given $j \rightarrow j'$ transition.[28,29]

A distinctive quasi-quantum treatment (QQT) is presented in the current study, where the l, l', and J quantum numbers are replaced by angular variables that provide a direct connection between the incoming and outgoing states and momenta. The present work builds on pioneering work of Hoffman,[30] who developed a classical kinetic theory for a mixture of dilute gases of rigid convex molecules. Molecular orientation variables, not impact parameters, were used to evaluate the collision integrals. Evans and co-workers[31,32] succeeded in extending Hoffman's angular parametrization to the calculation of the classical bimolecular rate constant, the energy-dependent reaction cross section, and the steric dependence of the differential cross sections for general diatom−diatom collisions. In the present study, we will exploit the l, l', J replacement by angular variables to gain understanding and to calculate differential cross sections and steric asymmetries for scattering on anisotropic (heteronuclear) potentials. The straightforward expressions derived in this way provide an intuitive basis for understanding the source of the observed steric asymmetry.

This paper is organized in six sections and Supporting Information. Section 2 describes the main ideas behind the QQT and applies it to both fully state-selected, nonoriented molecules (section 2A) and oriented molecules (section 2B). A previously unrecognized propensity rule for the differential cross section follows from this treatment. In section 3, a hard-shell approximation is introduced to obtain the molecule-fixed scattering amplitude. This scattering amplitude, which contains the phase shift, is necessary in order to obtain quantitative results from the QQT. The quantitative QQT results are discussed in section 4 and compared to experimental results. Some conclusions and a future outlook are given in section 5. In the Supporting Information, a short discussion is given concerning the impact the QQT has on the discrepancy in the sign of the steric asymmetry ratio.[7,11] This discussion directly relates to our results but is not the central focus of the present study.

2. Quasi-Quantum Treatment

The QQT aims at the simplification and approximation of exact quantum treatments. It presents an intuitive basis for understanding the physics behind the steric asymmetry and —

(19) Kramer, K. H.; Bernstein, R. B. *J. Chem. Phys.* **1964**, *40*, 200.
(20) Fenstermaker, R. W.; Bernstein, R. B. *J. Chem. Phys.* **1967**, *47*, 4417.
(21) Cross, R. J. *J. Chem. Phys.* **1968**, *49*, 1753.
(22) Curtiss, C. F. *J. Chem. Phys.* **1968**, *49*, 1952−1957.
(23) Pack, R. T. *J. Chem. Phys.* **1974**, *60*, 633−639.
(24) McGuire, P.; Kouri, D. J. *J. Chem. Phys.* **1974**, *60*, 2488.
(25) Dickenson, A. S.; Richards, D. *J. Phys. B* **1978**, *6*, 1085.
(26) Stolte, S.; Reuss, J. *Atom-Molecule Collision Theory: A Guide for the Experimentalist*; Plenum Press: New York, 1979; Chapter 5, p 201.
(27) Khare, V.; Kouri, D. J.; Hoffmann, D. K. *J. Chem. Phys.* **1981**, *74*, 2275.
(28) Khare, V.; Kouri, D. J.; Hoffmann, D. K. *J. Chem. Phys.* **1982**, *76*, 4493.
(29) Kouri, D. J.; Hoffman, D. K. *Theor. Chem. Acc.* **2000**, *103*, 281−285.
(30) Hoffman, D. K. *J. Chem. Phys.* **1969**, *50*, 4823−4831.
(31) Evans, G. T.; She, R. S. C.; Bernstein, R. B. *J. Chem. Phys.* **1985**, *682*, 2258−2266.
(32) She, R. S. C.; Evans, G. T.; Bernstein, R. B. *J. Chem. Phys.* **1986**, *84*, 2204−2211.

more generally — the relationship between inelastic collisions and the anisotropy of the intermolecular potential.

For scattering trajectories (rays) to interfere, the trajectories from a single initial state need to be scattered under an identical angle and into the same final molecular state. The impact parameter b gives the distance between a straight line along the trajectory of the incoming particle long before collision and the (center-of-mass) origin of the potential (see Figure 2). The orbital angular momentum before collision (with quantum number l) is fixed by $\boldsymbol{k}$ and the impact parameter b. Traditionally, to calculate differential cross sections, a summation over l is made that in the classical limit can be replaced by integration over $b \approx l/k$ (for example, see ref 15). For elastic (atom−atom) scattering on a Lennard-Jones type of potential, there are only three trajectories with different impact parameters that lead to the same scattering angle[33] and thus interfere. One of the three trajectories is mostly caused by the repulsive part of the potential, and the other two are due to the attractive part.[33]

In the case of an anisotropic potential, even when neglecting the attractive part, the repulsive part of the potential allows scattering into a certain angle for a range of impact parameters. This is demonstrated in Figure 2 using a hard egg-shaped potential. Solving this scattering problem numerically involves a large set of coupled (j, l, ϵ, j', l', ϵ') differential equations at each value of J, which makes these treatments time-consuming.[14,34] Calculating steric asymmetries for the He−NO collision system with current technology takes a set of several parallel processors several days.[12]

Approximations are introduced to reduce the size of the calculations. The projection m_a of the total angular momentum $\boldsymbol{j}$ on an apse $\hat{\boldsymbol{a}}$ is approximately conserved during the collision, when the repulsive part of the potential dominates (in the sudden approximation). Apse quantization was proposed and demonstrated to be a feasible approximation by Khare et al.[27,28,35] Later, Meyer et al. showed experimentally that the apse approximation yields good quantitative results for (among others) He−NO collisions[36] and Ne−NO collisions.[37] In this work, the kinematic apse will be used which — in contrast to the geometric apse — relies on the final rotational state. The kinematic apse is defined as[27]

$$\hat{\boldsymbol{a}}_k = \frac{\boldsymbol{k}' - \boldsymbol{k}}{|\boldsymbol{k}' - \boldsymbol{k}|} \tag{4}$$

The spherical angles which define the direction of the kinematic apse in the collision frame ($\hat{\boldsymbol{Z}} \equiv \hat{\boldsymbol{k}}$) are defined as β and α. The orientation of the molecular axis with respect to the kinematic apse is given by the spherical angles γ_a and ϕ_a.

In the QQT, the commonly used sum over l (or integral over the impact parameter b) is replaced by an integral over the apse angles β and α. The scattering angle ϑ is determined fully by the angle β of the kinematic apse with the incoming momentum and by the final rotational state. When one integrates over b, scattering into the same angle and thus interfering contributions originate from many values of b (see Figure 2), making the integral cumbersome to evaluate. Figure 3 schematically shows

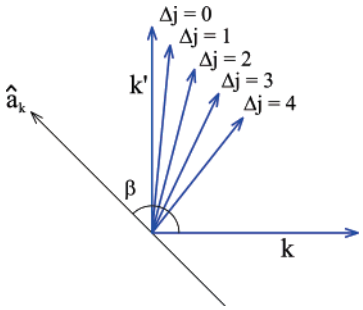

Figure 3. Part of the incoming momentum $\boldsymbol{k}$ is transformed into rotation. The orientation of the apse (β) and the translational energy loss due to rotational excitation Δj fixes the scattering angle.

the scattering angle of the outgoing momentum for different final rotational states at a *single* direction of the kinematic apse. Note that $^1/_2\pi \leq \beta \leq \pi$ for scattering with $k' \leq k$. No interfering contributions from different apse orientations occur, as there is a direct relationship between apse angle and scattering angle.

To find the relationship between the scattering angle (ϑ), the incoming momentum (k), and the angle between the apse and incoming momentum (β), the energy of each rotational level of the NO molecule $E(j)$ has to be known. The amount of kinetic energy that is converted into rotation is given by

$$E(j') = \frac{1}{2\mu}(|\boldsymbol{k} - \boldsymbol{k}'|)^2 \tag{5}$$

where μ is the reduced mass. The relationship between ϑ and β can be written explicitly as

$$\vartheta = \beta - \arctan\left(\frac{k \sin\beta}{k|\cos\beta| - \frac{1}{\hbar}\sqrt{2\mu E(j')}}\right) \tag{6}$$

In the experiments described in refs 3, 4, 6, and 13, the molecules are prepared in the upper component of the Λ-doublet of the rotational ground state ($j = {}^1/_2$, $\bar{\Omega} = {}^1/_2$, $\epsilon = -1$). In collisions with rare gas atoms, the NO molecules are excited to higher rotational states (j', $\bar{\Omega}'$, ϵ'). The spin−orbit constant A_0 and the rotational constant B_0 used to calculate the rotational energy of a NO molecule in the $v = 0$, $X^2\Pi$ state are $A_0 = 123.13\ \text{cm}^{-1}$ and $B_0 = 1.6961\ \text{cm}^{-1}$.[38]

In the current treatment, the attractive part of the rare gas−NO interaction will be neglected; the maximum well depth for He−NO and Ar−NO (25 and 116 cm^{-1}, respectively[39,40]) is much smaller than the kinetic energy, compared to a collision energy of $\sim$500 cm^{-1}. Only spin−orbit-conserving $\Omega' = \Omega$ transitions are considered. Spin−orbit-changing transitions are expected to be governed by the difference potential energy surface (PES) V_{diff},[8] which is not included in the present treatment.

The first goal is to calculate the state-to-state differential cross section, $d\sigma/d\omega$, which is — for a j, m, $\Omega \rightarrow j'$, m', Ω' transition — related to the dimensionless scattering amplitude by

(33) Pauly, H.; Toennies, J. P. *Neutral−Neutral Interactions*; Academic Press: New York, 1968; Vol. 7, Part A, p 227.
(34) Althorpe, S. C.; Clary, D. C. *Annu. Rev. Phys. Chem.* **2003**, *54*, 495.
(35) Khare, V.; Kouri, D. J.; Hoffmann, D. K. *J. Chem. Phys.* **1981**, *74*, 2656.
(36) Meyer, H. *J. Chem. Phys.* **1995**, *102*(8), 3151.
(37) Kim, Y.; Meyer, H.; Alexander, M. H. *J. Chem. Phys.* **2004**, *121*, 1339.
(38) Amiot, C. *J. Mol. Spectrosc.* **1982**, *94*, 150.
(39) Kłos, J.; Chalasinski, G.; Berry, M. T.; Kendall, R. A.; Burcl, R.; Szczesniak, M.; Cybulski, S. M. *J. Chem. Phys.* **2000**, *112*, 4952.
(40) Alexander, M. H. *J. Chem. Phys.* **1999**, *111*, 7426−7434.

$$\frac{d\sigma_{j,m,\Omega\rightarrow j',m',\Omega'}}{d\omega} = \frac{1}{k^2}|f_{j,m,\Omega\rightarrow j',m',\Omega}(\vartheta,\varphi)|^2 \quad (7)$$

The scattering amplitude is defined as the coefficient of the outgoing wave in

$$\Psi \propto \Psi_{j,m,\Omega}e^{i\boldsymbol{k}\cdot\boldsymbol{R}} + \sum_{j',m'}\Psi_{j',m',\Omega}\, f_{j,m,\Omega\rightarrow j',m',\Omega}(\vartheta,\varphi)\frac{ie^{ik'R}}{\sqrt{kk'}R} \quad (8)$$

In ref 41, it was shown that eq 2 is a proper asymptotic solution of the Schrödinger equation. Integration of the differential cross section over $d\omega = \sin\vartheta\, d\vartheta\, d\varphi$ provides the total cross section $\sigma_{j,m,\Omega\rightarrow j',m',\Omega}$.

The conventional scattering amplitude $f_{j,m,\Omega\rightarrow j',m',\Omega}(\vartheta)$ can be expressed in a newly introduced scattering amplitude $g_{j,m,\Omega\rightarrow j',m',\Omega}(\beta)$. The azimuthal angles α and φ are redundant because of cylindrical symmetry; note $\alpha = \varphi$. The scattering amplitudes are related via a Jacobian:

$$f_{j,m,\Omega\rightarrow j',m',\Omega}(\vartheta) = \sqrt{\frac{\sin\beta}{\sin\vartheta}\left|\frac{\partial\beta}{\partial\vartheta}\right|}\, g_{j,m,\Omega\rightarrow j',m',\Omega}(\beta) \quad (9)$$

Note that eq 9 does not specify the choice of the quantization axis. Recall that the projection of the total angular momentum on the apse (m_a) is (approximately) conserved during the scattering process ($m_a' = m_a$). Including m_a conservation in the calculation leads to an enormous simplification. The scattering amplitude in the apse frame (where the apse $\hat{\boldsymbol{a}}_k$ serves also as the quantization axis) is obtained by sandwiching a molecule-fixed scattering amplitude between the initial and final wave functions in the apse frame. An analogous equation — although not in the apse frame — can be found as eq 40 in ref 26.

$$\begin{aligned} g_{j,m_a,\Omega\rightarrow j',m_a,\Omega}(\beta) &= C(\beta)\langle j',m_a,\Omega|g_{j\rightarrow j'}(\gamma_a;\beta)|j,m_a,\Omega\rangle \\ &= C(\beta)\int_0^{\pi}\int_0^{2\pi}\Psi^*_{j',m_a,\Omega}\, g_{j\rightarrow j'}(\gamma_a;\beta)\, \Psi_{j,m_a,\Omega} \\ &\qquad \sin\gamma_a\, d\phi_a\, d\gamma_a \quad (10) \end{aligned}$$

For now we will proceed without quantifying the molecule-fixed scattering amplitude $g_{j\rightarrow j'}(\gamma_a;\beta)$ that connects the incoming and outgoing wave functions and carries their phase shifts. $C(\beta)$ is a normalization factor that is discussed in detail later (see eq 18). The angle γ_a of the molecular axis $\boldsymbol{r}$ with the apse $\hat{\boldsymbol{a}}_k$ is assumed to be fixed during the collision. In section 3, a hard-shell potential will be used to approximate $g_{j\rightarrow j'}(\gamma_a;\beta)$, but there is no restriction to such a potential. The absolute value of the molecule-fixed scattering amplitude is taken as the square root of the apse-dependent classical differential cross section, $d\sigma/d\omega_a \equiv d\sigma/\sin\beta\, d\beta\, d\alpha$, which is independent of the final rotational state.

$$|g_{j\rightarrow j'}(\gamma_a;\beta)| = k\sqrt{\frac{\partial^2\sigma(\gamma_a)}{|\sin(\beta)\,\partial\beta|\partial\alpha}} \quad (11)$$

The integration of eq 10 contains the product of the initial and (complex conjugate of) the final wave functions. The rotational wave function can be expressed as[42]

$$\begin{aligned} \Psi_{j,m_a,\Omega} &= \sqrt{\frac{2j+1}{4\pi}}D^{j*}_{m_a,\Omega}(\phi_a,\gamma_a,0) \\ &= (-1)^{m_a-\Omega}\sqrt{\frac{2j+1}{4\pi}}D^{j}_{-m_a,-\Omega}(\phi_a,\gamma_a,0) \quad (12) \end{aligned}$$

The product of the wave functions that appears in the integral of eq 10 can — after using eq 3.116 of ref 42 — be contracted to

$$\Psi^*_{j',m_a,\Omega}\Psi_{j=1/2,m_a,\Omega} = \frac{1}{4\pi}\sqrt{j'+1/2}\left[P_{j'-1/2}(\cos\gamma_a) + \frac{m_a\Omega}{\overline{m_a\Omega}}P_{j'+1/2}(\cos\gamma_a)\right] \quad (13)$$

Here, $\overline{m_a\Omega}$ denotes the absolute value of the product $m_a\Omega$. We apply this result first to fully state-selected molecules (as in ref 13) and after that to oriented molecules.

A. State-Selected Molecules. The pure parity wave function for an NO molecule in the apse frame (neglecting Hund case *b* mixing) can be written as

$$|j,m_a,\bar{\Omega},\epsilon\rangle = \frac{1}{\sqrt{2}}[|j,m_a,\bar{\Omega}\rangle + \epsilon|j,m_a,-\bar{\Omega}\rangle] \quad (14)$$

The parity of a wave function is defined by its behavior under parity transformation (inversion), which acts as a unitary operator $\boldsymbol{P}$ on a wave function ψ:

$$\boldsymbol{P}\psi(\boldsymbol{r}) = \psi(-\boldsymbol{r}) = p\psi(\boldsymbol{r}) \quad (15)$$

The total parity p of a rotational state (eigenvalue of $\boldsymbol{P}$) is provided by Brown et al.:[43]

$$p = (-1)^{j-\epsilon/2} \quad (16)$$

Using the result in eq 13, the differential cross section for scattering of $j = 1/2$, $\bar{m}_a = 1/2$, $\bar{\Omega} = 1/2$, $\epsilon \rightarrow j'$, $\bar{m}_a = 1/2$, $\bar{\Omega} = 1/2$, ϵ' is given by

$$\frac{d\sigma_{j=1/2,\epsilon\rightarrow j',\epsilon'}}{d\omega} = C(\beta)^2\frac{j'+1/2}{4k^2}\frac{\sin\beta}{\sin\vartheta}\left|\frac{\partial\beta}{\partial\vartheta}\right||\, g_{j'-\epsilon\epsilon'/2}(\beta)|^2 \quad (17)$$

with

$$g_n(\beta) = \int_{-1}^{1} g_{j\rightarrow j'}(\gamma_a;\beta)P_n(\cos\gamma_a)\mathrm{d}\cos(\gamma_a)$$

To enhance the readability, subscripts indicating the conserved quantum numbers m_a and $\bar{\Omega}$ are suppressed.

The factor $C(\beta)$ takes care of current density conservation along the kinematic apse, which lies along the direction of momentum transfer. The total differential cross section with respect to the apse (summed over all rotational states) for inelastic scattering has to be the same as its classical counterpart:

(41) Lester, W. A. *Methods in Computational Physics*; Academic Press: New York, 1971; Vol. 10.

(42) Zare, R. N. *Angular Momentum: Understanding spatial aspects in chemisty and physics*; John Wiley & Sons: New York, 1988.

(43) Brown, J. M.; Hougen, J. T.; Huber, K. P.; Johns, J. W. C.; Kopp, I.; LeFebvre-Brion, H.; Merer, A. J.; Ramsay, D. A.; Rostas, J.; Zare, R. N. *J. Mol. Spectrosc.* **1975**, *55*, 500.

$$C(\beta)^2 = \frac{d\sigma_{class}}{d\omega_a} \Big/ \sum_{j',\epsilon'} \frac{j' + {}^1/_2}{4k^2} |g_{j'-\epsilon\epsilon'/2}(\beta)|^2 \quad (18)$$

with

$$\frac{d\sigma_{class}}{d\omega_a} = \int_0^{2\pi}\int_0^{\pi} \Psi^*_{j,m_a,\bar{\Omega},\epsilon} \Psi_{j,m_a,\bar{\Omega},\epsilon} \frac{d\sigma(\gamma_a;\beta)}{d\omega_a} \sin\gamma_a \, d\gamma_a \, d\phi_a \quad (19)$$

Recall that

$$d\omega_a = \sin\beta \, d\beta \, d\varphi \quad (20)$$

In the case of $j = {}^1/_2$, eq 19 can be simplified as

$$\frac{d\sigma_{class}}{d\omega_a} = \frac{1}{4\pi}\int_0^{2\pi}\int_0^{\pi} \frac{d\sigma(\gamma_a;\beta)}{d\omega_a} \sin\gamma_a \, d\gamma_a \, d\phi_a \quad (21)$$

The effect of the weak j' dependence of the phase shift in $g_{j\rightarrow j'}(\gamma_a;\beta)$ for neighboring j' values is suppressed for the remainder of section 2, and $g_{j\rightarrow j'}(\gamma_a;\beta)$ is abbreviated as $g(\gamma_a;\beta)$. In eq 17, it can be seen that the differential cross sections for transitions from $j = {}^1/_2$, $\epsilon = -1$ to two neighboring rotational states with the same parity (for example, $j' = {}^7/_2$, $\epsilon' = 1$ and $j' = {}^9/_2$, $\epsilon' = -1$) are similar, except for a different prefactor ($j' + {}^1/_2$). This propensity rule immediately follows from eq 17:

$$\frac{d\sigma_{{}^1/_2,\epsilon=-1\rightarrow{}^3/_2,\epsilon'=1}}{d\omega} \approx \frac{2}{3} \frac{d\sigma_{{}^1/_2,\epsilon=-1\rightarrow{}^5/_2,\epsilon'=-1}}{d\omega} \propto \left|\int_{-1}^{1} g(\gamma_a;\beta) \, P_2(\cos\gamma_a) \, d\cos(\gamma_a)\right|^2$$

$$\frac{d\sigma_{{}^1/_2,\epsilon=-1\rightarrow{}^5/_2,\epsilon'=1}}{d\omega} \approx \frac{3}{4} \frac{d\sigma_{{}^1/_2,\epsilon=-1\rightarrow{}^7/_2,\epsilon'=-1}}{d\omega} \propto \left|\int_{-1}^{1} g(\gamma_a;\beta) \, P_3(\cos\gamma_a) \, d\cos(\gamma_a)\right|^2$$

$$\frac{d\sigma_{{}^1/_2,\epsilon=-1\rightarrow{}^7/_2,\epsilon'=1}}{d\omega} \approx \frac{4}{5} \frac{d\sigma_{{}^1/_2,\epsilon=-1\rightarrow{}^9/_2,\epsilon'=-1}}{d\omega} \propto \left|\int_{-1}^{1} g(\gamma_a;\beta) \, P_4(\cos\gamma_a) \, d\cos(\gamma_a)\right|^2$$

et cetera.

The current treatment explains the surprising observation that differential cross sections come in "parity pairs", as seen in ion imaging (velocity mapping) experiments.[13] Ion images of product angular distributions for spin−orbit-conserving He−NO collisions are plotted in Figure 4. The top panel displays images for parity-conserving transitions, while the lower panel shows images for parity-breaking transitions. The "parity pairs" for each final rotational state with identical $j' - \epsilon\epsilon'/2$ are grouped in this figure and spaced from the other images. The intensity in the ion images reflects the two-dimensional velocity distribution of the NO molecules after collision with a He atom. The intensity on an outer ring roughly reflects the differential cross section. For excitation to low j', the NO molecules are mostly scattered in the forward direction, whereas for high final rotational states, backward scattering is preferred. This can easily be understood. Glancing collisions — where little translational energy is transformed into rotational energy — are forward scattered, whereas head-on collisions allow for higher rotational states and will show mostly backward scattering.

Although the ion images of Figure 4 clearly show the presence of parity pairs, these images remain unable to give information on the absolute value of the differential cross sections. To test the predicted (prefactor) ratios between the differential cross section within the pairs, these ratios are compared to those obtained from quantum-mechanical coupled channel (HIBRIDON)[9] calculations.[13] The ratios A_n between HIBRIDON differential cross sections within parity pairs are obtained with a least-squares fit, where

$$\int_0^{\pi} \left[\frac{d\sigma}{d\omega}\Big|_{\Delta j=n+1} - A_n \frac{d\sigma}{d\omega}\Big|_{\Delta j=n}\right]^2 d\vartheta \quad (\text{with } n = 1, 2, 3, ...) \quad (22)$$

is minimized. The resulting close-coupling ratios are compared to those from the QQT prefactors in Table 1. For low final rotational states, there exists a good qualitative agreement with the ratios predicted from eq 17, although for the highest rotational states the agreement is reduced. Until now, no thorough explanation for the disagreement at high rotational states has been available, but at this region the contribution of spin−orbit-changing collisions becomes comparable to that of spin−orbit-conserving collisions. Additionally, the angular dependence of the differential cross sections turns out to be more distinctive for large j'.[13]

The contra-intuitive result that the differential cross section to the upper j' component of each parity pair $j' - \epsilon\epsilon'/2$ is larger than that to the lower j' component opposes the "exponential gap" model.[2,44] This rule of thumb predicts that the cross section for a small "gap" (the change of translational energy during collision) and thus a small j' is larger than that to a higher one.

Application of classical **S**-matrix theory showed that collisions between rare gas atoms and nearly homonuclear $^1\Sigma$ molecules favor rotational transitions with Δj even.[45] This propensity rule cannot simply be extended to collisions of $^2\Pi$ molecules like NO. Each rotational j state carries both parities in the two components of the Λ-doublet. In this work, as well as in that by Drabbels et al.,[46] the preference of Δj for conservation or breaking of parity was studied. For parity-conserving collisions of He with NO, it was observed that, for $\Delta j \leq 4$, transitions with Δj even are preferred, while for parity-breaking transitions both studies find a preference for Δj odd transitions. The $(2j' + 1)$ prefactor in eq 17 explains both propensities.

B. Oriented Molecules. The result in eq 13 is applied to oriented molecules in this subsection. Under the influence of a static electric orientation field **E**, the hexapole state-selected wave function can be described as a linear combination of both components of the Λ-doublet:[7]

$$|j,m,\bar{\Omega},E\rangle = \alpha(E)|j,m,\bar{\Omega},\epsilon = -1\rangle \pm \beta(E)\frac{m}{\bar{m}}|j,m,\bar{\Omega},\epsilon = 1\rangle \quad (23)$$

The $\pm$ indicates orientation. For "+" orientation there is preference for $\boldsymbol{r}$ to point parallel to the quantization axis ($\boldsymbol{r}^{\uparrow\uparrow}\hat{\boldsymbol{Z}}$), while for "−" orientation these vectors point antiparallel ($\boldsymbol{r}^{\uparrow\downarrow}\hat{\boldsymbol{Z}}$).

The parameters $\alpha(E)$ and $\beta(E)$ in eq 23 are the mixing coefficients. If the orientation field cannot be assumed to be infinitely high, mixing is not complete and $\alpha(E) > \beta(E) > 0$, with $\alpha^2 + \beta^2 = 1$. For an infinitely high orientation field $\mathbf{E}_\infty$,

(44) Joswig, H.; Andresen, P.; Schinke, R. *J. Chem. Phys.* **1986**, *85*, 1904.
(45) McCurdy, C. W.; Miller, W. H. *J. Chem. Phys.* **1977**, *67*, 463.
(46) Drabbels, M.; Wodtke, A. M.; Yang, M.; Alexander, M. H. *J. Phys. Chem. A* **1997**, *101*, 6463.

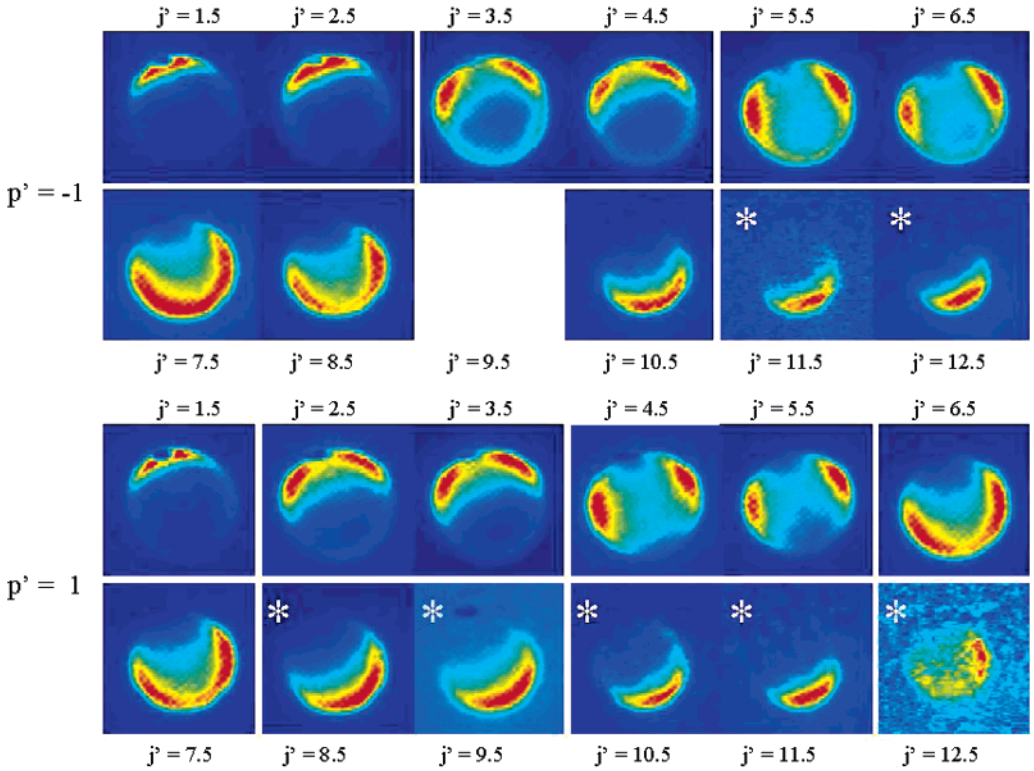

Figure 4. Ion images for He−NC collisions at $E_{tr} = 514$ cm^{-1}. Marked images (*) are from P+Q or Q+R branch transitions. These images are more sensitive to collision-induced rotational alignment and therefore show more asymmetry than those from single P and R branches.[13] The parity pairs are grouped and separated from the other images by white lines. The image for $p' = -1$, $j' = 9.5$ could not be obtained because of two overlapping spectral lines. Images for $p' = 1$, $j' = 6.5$ and $p' = 1$, $j' = 7.5$ form a pair as well, although they are displayed on different rows.

Table 1. Parity Pairs for He−NO Collisions[a]

		$(d\sigma/d\omega)\|_{\Delta j=n+1}/(d\sigma/d\omega)\|_{\Delta j=n}$		
n	p'	QQT prefactor		A_n (CC HIBRIDON)
1	1	3/2	1.50	1.54
2	−1	4/3	1.33	1.36
3	1	5/4	1.25	1.23
4	−1	6/5	1.20	1.30
5	1	7/6	1.17	1.16
6	−1	8/7	1.14	1.25
7	1	9/8	1.13	1.13
8	−1	10/9	1.11	1.07
9	1	11/10	1.10	1.32
10	−1	12/11	1.09	0.88
11	1	13/12	1.08	2.50

[a] A least-squares method was used to find ratios between differential cross sections from quantum calculations. For the QQT the ratios between the prefactors ($j' + 1/2$) are provided. The ratio between the differential cross sections for the QQT might be slightly different due to the dependence of the phase shift on the final rotational state.

$\alpha(E) = \beta(E) = 1/\sqrt{2}$, the wave function can then be written as We first focus on this simpler case. Substitution of eq 14 into

$$|j,m,\bar{\Omega},E_\infty\rangle = \frac{1}{\sqrt{2}}\left[|j,m,\bar{\Omega},\epsilon=-1\rangle \pm \frac{m}{\bar{m}}|j,m,\bar{\Omega},\epsilon=1\rangle\right] \quad (24)$$

24 now yields

$$|j,m,\bar{\Omega},E_\infty\rangle = \left|j,m,\Omega=\frac{m}{\bar{m}}\bar{\Omega}\right\rangle \quad \text{for "+" orientation}$$
$$|j,m,\bar{\Omega},E_\infty\rangle = -\left|j,m,\Omega=-\frac{m}{\bar{m}}\bar{\Omega}\right\rangle \quad \text{for "−" orientation} \quad (25)$$

For convenience, the orientation is for now taken relative to the apse; m in eqs 24 and 25 is replaced by m_a:

$$|j,m_a,\bar{\Omega},E_\infty\rangle = \left|j,m_a,\Omega=\frac{m_a}{\bar{m}_a}\bar{\Omega}\right\rangle \quad \text{for "+" orientation} \quad (26)$$

$$|j,m_a,\bar{\Omega},E_\infty\rangle = -\left|j,m_a,\Omega=-\frac{m_a}{\bar{m}_a}\bar{\Omega}\right\rangle \quad \text{for "−" orientation} \quad (27)$$

Recall that orientation is defined such that for "+" orientation the molecular axis ***r*** preferentially is parallel to the quantization axis, while for "−" orientation it preferentially is antiparallel. It should be noted that, in eq 27, the apse serves as quantization axis $\hat{\boldsymbol{Z}} = \hat{\boldsymbol{a}}$. In NO, ***r*** points from the O atom toward the N atom. In the apse frame, the "+" orientation relates to an R−NO collision geometry and the "−" orientation to an R−ON geometry. Transformation from the apse frame to the collision frame — which weakens the orientation effects — will be done at a later stage. The orientation-dependent scattering amplitude in the apse frame follows directly from the substitution of eq 13 in eq 10:

$$g_{1/2,\pm\to j'}(\beta) = \pm C(\beta)\frac{1}{2}\sqrt{j'+1/2}\,[g_{j'-1/2}(\beta) \pm g_{j'+1/2}(\beta)] \quad (28)$$

with

$$g_n(\beta) = \int_{-1}^{1} g_{j\to j'}(\gamma_a;\beta)P_n(\cos\gamma_a)\,\mathrm{d}\cos(\gamma_a)$$

This equation turns out to be very helpful in explaining the

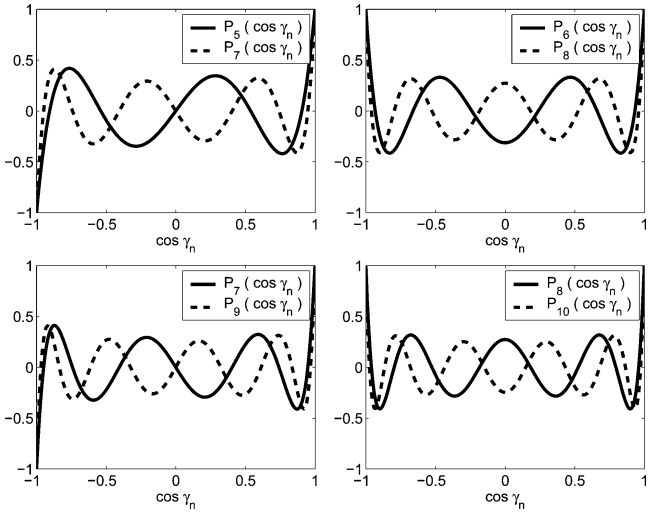

Figure 5. Example of Legendre polynomials. Roughly speaking, $P_n(\cos \gamma_a) \approx -P_{n+2}(\cos \gamma_a)$ in the (broad) region around $\cos \gamma_a = 0$.

oscillations of the steric asymmetry S as a function of the final rotational state.

To obtain a relationship between the relevant scattering amplitudes, the recurrence relationship for Legendre polynomials will be used:

$$P_{n+1}(x) = \frac{2n+1}{n+1}\, x\, P_n(x) - \frac{n}{n+1}\, P_{n-1}(x) \qquad (29)$$

For large n this reduces to

$$P_{n+2}(x) \approx 2xP_{n+1}(x) - P_n(x) \qquad (30)$$

Around the center ($x \approx 0$), $P_n(x)$ dominates in eq 30. At the edges ($|x| \approx 1$), $2x\, P_{n+1}(x)$ dominates. Overall, both terms are equally important as P_{n+1} is multiplied with $2x$ ($-1 < x < 1$). Note that the amplitude of the oscillations of $P_{n+1}(x)$ is only slightly smaller than that of $P_n(x)$. In Figure 5, some Legendre polynomials are plotted to illustrate that $P_{n+2}(x) \approx -P_n(x)$ around $x \approx 0$.

Substitution of eq 30 into eq 28 gives

$$g_n(\beta) \approx -g_{n+2}(\beta) + 2\int_{-1}^{1} g_{j\rightarrow j'}(\gamma_a;\beta) \cos \gamma_a\, P_{n+1}(\cos \gamma_a)\, \mathrm{d}\cos(\gamma_a) \qquad (31)$$

If the contributions around the waist of the molecules ($\cos \gamma_a = 0$) dominate the integral, the second term in eq 31 can be neglected: $g_n(\beta) \approx -g_{n+2}(\beta)$. This will be the case when the phase shift η close to $\cos \gamma_a = 0$ is stationary:[15] i.e., η does not depend on $\cos \gamma_a$, which is expected for a prolate molecule like NO. Under these conditions, it is easily shown why the orientation preference switches sign when increasing $j' \rightarrow j' + 1$. The $\pm$ orientation-dependent differential cross section for excitation to j' immediately follows from eq 28:

$$\frac{\mathrm{d}\sigma_{1/2,\pm\rightarrow j'}}{\mathrm{d}\omega} = \frac{j' + {}^1\!/_2}{4k^2} C(\beta)^2 \frac{\sin \beta}{\sin \vartheta}\left|\frac{\partial \beta}{\partial \vartheta}\right| \left| g_{j'-1/2}(\beta) \pm g_{j'+1/2}(\beta)\right|^2 \qquad (32)$$

For $j' + 1$, this results in

$$\frac{\mathrm{d}\sigma_{1/2,\pm\rightarrow j'+1}}{\mathrm{d}\omega} = \frac{j' + {}^3\!/_2}{4k^2} C(\beta)^2 \frac{\sin \beta}{\sin \vartheta}\left|\frac{\partial \beta}{\partial \vartheta}\right| \left| g_{j'+1/2}(\beta) \pm g_{j'+3/2}(\beta)\right|^2 \qquad (33)$$

Substitution of $g_{n+2}(\beta) \approx -g_n(\beta) \rightarrow g_{j'+3/2}(\beta) \approx -g_{j'-1/2}(\beta)$ yields Comparing the right-hand sides of eqs 32 and 34, one notices

$$\frac{\mathrm{d}\sigma_{1/2,\pm\rightarrow j'+1}}{\mathrm{d}\omega} \approx \frac{j' + {}^3\!/_2}{4k^2} C(\beta)^2 \frac{\sin \beta}{\sin \vartheta}\left|\frac{\partial \beta}{\partial \vartheta}\right| \left| g_{j'-1/2}(\beta) \mp g_{j'+1/2}(\beta)\right|^2 \qquad (34)$$

that they are nearly similar, except for the prefactor and the $\pm$ in the integral, which defines the orientation. The $\pm$ is exchanged for a $\mp$, which implies that the orientation preference is reversed when increasing $j' \rightarrow j' + 1$.

Incomplete mixing due to finite field strength can be included in the model. Application of eq 23 as the initial wave function leads to the orientation-dependent differential cross section:

$$\frac{\mathrm{d}\sigma_{1/2,\pm,E\rightarrow j',\epsilon'}}{\mathrm{d}\omega} = \frac{j' + {}^1\!/_2}{4k^2} C(\beta)^2 \frac{\sin \beta}{\sin \vartheta}\left|\frac{\partial \beta}{\partial \vartheta}\right| \left|\alpha(E) g_{j'+\epsilon'/2}(\beta) \pm \beta(E) g_{j'-\epsilon'/2}(\beta)\right|^2 \qquad (35)$$

The observed steric asymmetry will, in practice, be smaller than what follows from integration of eq 35. Recall that orientation has been, until now, defined along the apse: the product $m_a\Omega$ gives the orientation, where m_a is the projection of $\boldsymbol{j}$ on the apse. In experiments, molecules are oriented along an electric field that is usually fixed in the laboratory.

The projection of the total angular momentum on the $\hat{\boldsymbol{Z}}$-axis of the collision frame (parallel or antiparallel to the electric field $\boldsymbol{E}$) is defined by $m\Omega$ instead of $m_a\Omega$, where m is the projection of $\boldsymbol{j}$ on the $\hat{\boldsymbol{Z}}$-axis that points along the relative velocity. The final result is a linear combination of "+" and "−" orientation along the apse, weighted by the axis distribution of the selected state. There will be a weakening of the steric asymmetry from the pure apse-oriented state, but the conclusions drawn earlier on the undulating behavior of S remain intact. The laboratory and apse frames are related by rotation[42] through the polar angle β:

$$|j,m,\Omega\rangle = \sum_{m_a} \mathrm{d}^j_{m_a,m}(\beta)|j,m_a,\Omega\rangle \qquad (36)$$

In the scattering experiments with oriented NO molecules, the initial state is $j = {}^1\!/_2$. The differential cross section follows as where $m\Omega/\overline{m\Omega} = 1$ provides an R−ON configuration and

$$\frac{\mathrm{d}\sigma_{j=1/2,m\Omega=\pm 1/4,E\rightarrow j',\epsilon'}}{\mathrm{d}\omega} = \sin^2\!\left(\frac{\beta}{2}\right)\frac{\mathrm{d}\sigma_{j=1/2,m_a\Omega=\mp 1/4,E\rightarrow j',\epsilon'}}{\mathrm{d}\omega} + \cos^2\!\left(\frac{\beta}{2}\right)\frac{\mathrm{d}\sigma_{j=1/2,m_a\Omega=\pm 1/4,E\rightarrow j',\epsilon'}}{\mathrm{d}\omega} \qquad (37)$$

$m\Omega/\overline{m\Omega} = -1$ gives an R−NO configuration in the collision frame with $\hat{\boldsymbol{Z}} = \hat{\boldsymbol{k}}$. Note that $90° \le \beta \le 180°$, which implies that the first term with $\sin^2(\beta/2)$ is the strongest one. The "+" orientation in the collision frame is dominated by the "−" orientation in the apse frame because the quantization axis in the apse frame ($\hat{\boldsymbol{Z}} = \hat{\boldsymbol{a}}$) generally points opposite to that in the collision frame ($\hat{\boldsymbol{Z}} = \hat{\boldsymbol{k}}$). As low final rotational states are usually due to forward scattering (where $\beta \approx 90°$), it becomes clear

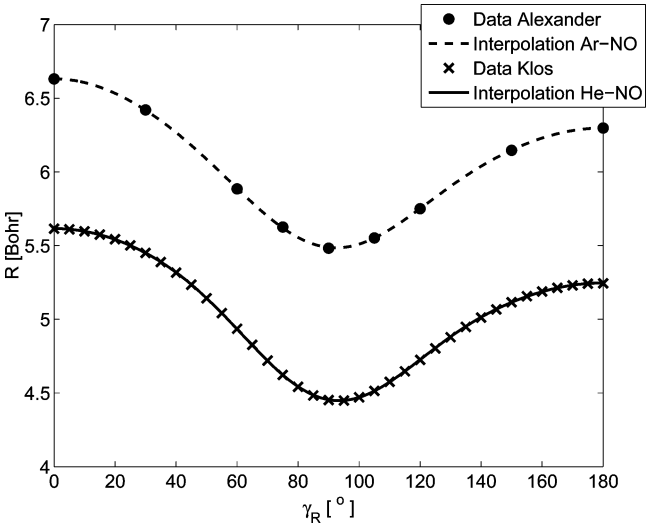

Figure 6. Calculated equipotential line and interpolation for NO−Ar, E_{tr} = 475 cm^{-1},[40] and NO−He PESs, E_{tr} = 514 cm^{-1}.[39] Coefficients from Table 2 are used. Note that $\gamma_R = 0$ corresponds to the R−NO configuration, while $\gamma_R = 180°$ corresponds to the R−ON configuration. The interpolation for Ar−NO is based on 9 data points, and that for He−NO is based on 37 points.

from eq 37 why the steric asymmetry has a small amplitude for low final rotational states. In this case, the two orientations in the apse frame ($m_a\Omega = \mp 1/4$ and $m_a\Omega = \pm 1/4$) are approximately equally important for the two orientations in the laboratory frame: $\cos^2(\beta/2) \approx \sin^2(\beta/2)$ if $\beta \approx 90°$.

3. Hard-Shell Approximations

To be able to calculate differential and integral cross sections, it is necessary to provide an explicit expression for the molecule-fixed scattering amplitude $g_{j\rightarrow j'}(\gamma_a;\beta)$ that contains the phase shift. In this section, a hard-shell potential is applied to obtain $g_{j\rightarrow j'}(\gamma_a;\beta)$. The use of more sophisticated potential energy surfaces — soft and/or including attraction — is not treated here. At our collision energy, the He−NO and Ar−NO potential energy surfaces are reasonably well described in a hard-shell approximation. The aim of this work is to obtain a better insight into the physics of inelastic scattering.

The convex hard shell for Ar colliding with NO is approximated using the 475 cm^{-1} equipotential surface from Alexander's V_{sum} PESs.[40] The shell for He−NO uses the 514 cm^{-1} equipotential surface from V_{sum} PESs calculated by Kłos.[47] These equipotential surfaces are taken at the collision energies from refs 4, 6, and 13. The hard-shell Ar−NO and He−NO potentials are shown in Figure 6. As the amount of available ab initio points on the equipotential is limited, an interpolation has been used to establish the shell. The equipotential lines are expressed in a Legendre expansion:

$$R_s(\gamma_R) = \sum_{n=0}^{n_{max}} c_n P_n(\cos\gamma_R) \qquad (38)$$

In this equation, γ_R is the polar angle between the position vector of the shell and the molecular axis, while $R_s(\gamma_R)$ gives the distance from the origin of the potential to the hard shell (see also Figure 7). The coefficients for this expansion have been

(47) Kłos, J.; Chalasinski, G.; Berry, M. T.; Bukowski, R.; Cybulski, S. M. *J. Chem. Phys.* **2000**, *112*, 2195.

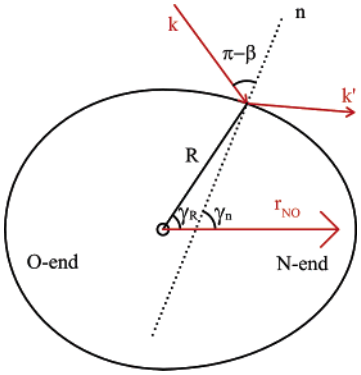

Figure 7. Schematic representation of a hard convex shell.

Table 2. Hard-Shell Legendre Polynomial Approximation Coefficients As Used in Eq 38

	c_n (Bohr)	
n	for He–NO hard shell	for Ar–NO hard shell
0	4.8637	5.8692
1	0.1983	0.1516
2	0.6908	0.6771
3	−0.0126	0.0142
4	−0.1497	−0.0999
5	−0.0012	0.0010
6	0.0263	0.0183

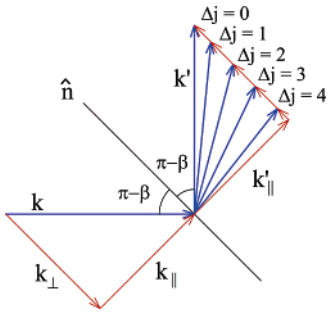

Figure 8. Assuming a hard shell, the scattering angle is defined by only the incoming momentum, the surface normal $\hat{n}$ (that coincides with the kinematic apse $\hat{\boldsymbol{a}}_k$) and the final rotational state.

calculated using a least-squares optimization routine. For Ar−NO, 9 points were supplied and used for the fit, while for He−NO the fit was made using 37 points. The c_n coefficients resulting from a fit to the expansion with $n_{max} = 6$ are shown in Table 2. As is shown in Figure 6, both the He−NO and the Ar−NO ab initio equipotential surfaces are excellently described using eq 38 with the fitted c_n constants of Table 2.

The surface normal $\hat{n}$ — that points perpendicularly to the hard shell — coincides with the kinematic apse $\hat{\boldsymbol{a}}_k$. In the hard-shell approximation, the scattering angle is determined only by the incoming momentum, the surface normal, and the final rotational state. This is demonstrated in Figure 8, where the incoming momentum $\boldsymbol{k}$ is decomposed in components parallel ($\boldsymbol{k}_{||}$) and perpendicular ($\boldsymbol{k}_{\perp}$) to the shell. The force that induces the rotation points perpendicular to the shell. The component of the momentum perpendicular to the hard shell is reversed and partly transformed into rotation. The component along the hard shell, $\boldsymbol{k}_{||}$ is conserved: $\boldsymbol{k}'_{||} = \boldsymbol{k}_{||}$.

The hard shells can be exploited to find the molecule-fixed scattering amplitude. This amplitude for a specific rotational excitation is written as

$$g_{j\rightarrow j'}(\gamma_a;\beta) = g_{\text{class}}(\gamma_a;\beta)\, e^{i\eta(\gamma_a;\beta)} \tag{39}$$

The $j \rightarrow j'$ dependent phase shift is denoted by $\eta(\gamma_a;\beta)$, and $g_{\text{class}}(\gamma_a;\beta)$ is a "classical" hard-shell scattering amplitude that follows from the classical differential cross section in the apse frame. For a spherical potential, g_{class} reduces to the square root of the classical differential cross section (in the apse frame):

$$g_{\text{class}}(\beta) = kR_s\sqrt{|\cos\beta|} \tag{40}$$

In this case, R_s is independent of the position on the hard shell ($\gamma_R = \gamma_a$). Integration of eq 10 for elastic scattering — $d\eta(\gamma_a;\beta)/d\gamma_a = 0$ or a constant as a function of γ_a — now yields the classical integral cross section:

$$\frac{1}{k^2}\int_{-1}^{0}\int_{0}^{2\pi}\left[kR_s\sqrt{|\cos\beta|}\,\right]^2 d\alpha\, d\cos\beta = \pi R_s^{\,2}$$

Note that, in this spherical shell approximation, the current density conservation parameter $C(\beta)$ reduces to

$$C(\beta)^2 = R_s^{\,2}|\cos\beta|\left|\sum_{j',\epsilon'}\frac{j'+{}^1\!/_2}{4k^2}|g_{j'-\epsilon\epsilon'/2}(\beta)|^2\right. \tag{41}$$

To calculate the phase shift $\eta(\gamma_a;\beta) \equiv (\boldsymbol{k} - \boldsymbol{k'})\cdot\boldsymbol{R}_s$, the hard convex potential is used. The phase shift is defined as the path length difference between a path via the hard shell and the corresponding imaginary path through the origin of the potential (center-of-mass), divided by the local de Broglie wavelength and multiplied by 2π:

$$\eta(\gamma_a;\beta) = -R_s(\gamma_R)\cos(\gamma_a - \gamma_R)(k'_\perp + k_\perp) \tag{42}$$

As $k_\perp = |k\cos\beta|$, it is easily seen that for a glancing collision the phase shift is zero, while for a head-on collision the absolute value of the phase shift is at a maximum.

Equation 42 contains both γ_R and γ_a. In Figure 7, it is shown that — unlike for a spherical shell — the angle γ_a between the normal (apse) $\hat{\boldsymbol{a}}_k$ and the molecular axis is not the same as the angle γ_R between $\boldsymbol{R}_s(\gamma_R)$ and the molecular axis.

A unique relationship between γ_R and γ_a follows if one transforms the hard-shell $R_s(\gamma_R)$ into cylinder coordinates (z,r): As the apse is perpendicular to the hard shell, one gets

$$z = R_s(\gamma_R)\cos(\gamma_R) \qquad \text{and} \qquad r = R_s(\gamma_R)\sin(\gamma_R) \tag{43}$$

$$\gamma_a = -\arctan\frac{dr}{dz} \tag{44}$$

Please note that z represents in this particular case a position on the molecular axis.

The expression for $g_{\text{class}}(\gamma_a;\beta)$ (eq 11) is no longer given by eq 40. Areas on the molecular shell that have a large radius of curvature will contribute more to the scattering amplitude than those with a small radius of curvature. By using the two radii of curvature ρ_1 and ρ_2 that support the differential surface dS as a function of γ_a and substituting their product for R_s^2 in eq 40, one obtains

$$g_{\text{class}}(\gamma_a;\beta) = \sqrt{\rho_1\rho_2|\cos\beta|} \tag{45}$$

The radii of curvature ρ_1 and ρ_2 are calculated as

$$\rho_1 = \frac{dC_f}{d\gamma_a} \tag{46}$$

$$\rho_2 = \frac{R_s(\gamma_R)\sin(\gamma_R)}{\sin(\gamma_a)} \tag{47}$$

$dC_f/d\gamma_a$ is the γ_a derivative of the arc length of the hard shell in a plane through the molecular axis. The second radius of curvature, ρ_2, is given by the distance from the molecular axis to the hard shell along the surface normal. Note that $g_{\text{class}}(\gamma_a;\beta)$ is the square root of the molecule-fixed differential cross section $d\sigma/d\omega_a$ with respect to the apse. With these results, the treatment can be applied to provide quantitative results. This is the subject of the next section.

4. Quantitative Results and Discussion

The general QQT of section 2 provides already some qualitative conclusions. In section 2.1, it was shown that the differential cross sections for collisions with fully state-selected (nonoriented) molecules show parity pairs and propensity rules. In section 2.2, it is argued why the steric asymmetry exhibits an oscillatory behavior as a function of the final rotational state. The calculation of the molecule-fixed scattering amplitude obtained from the hard-shell approximation makes it possible to obtain quantitative results. In this section, the hard-shell QQT will be applied to He−NO scattering to result in calculated angle-dependent differential cross sections for nonoriented molecules and steric asymmetries for collisions of He and Ar atoms with oriented molecules.

Upon substitution of eqs 42 and 45 into eqs 35 and 37, and subsequent evaluation of the integral, the differential cross section is obtained. Integration of the differential cross section leads to a cross section that, using eq 1, provides the steric asymmetry S. S is plotted in Figures 9 and 10 for two cases: He−NO with $\epsilon' = 1$ and Ar−NO with $\epsilon' = -1$. Mixing is not complete, so slightly more NO with $\epsilon = -1$ is present than that with $\epsilon = 1$ before collisions. Mixing coefficients were taken from ref 6 for He−NO and from ref 4 for Ar−NO. The QQT results for S correspond remarkably well to the measured steric asymmetries and coupled channel calculations. The experimental results are not shown in Figures 9 and 10 for readability, but (except for the unresolved sign error[7,11]) they correspond well to the exact (CC) values of S that are in the plot (see also Figure 1). The amplitude of S for scattering to the $\epsilon = -1$ state is smaller than that for scattering to $\epsilon = 1$. CC calculations and experimental results show the same behavior.

In eqs 32 and 34, it was shown that S shows an undulating behavior as a function of the final rotational quantum state j'. These equations, however, give no information about the sign of the oscillation. To get information on the sign of the steric asymmetry, the phase shift has to be included. In Figure 11, the phase shift (He−NO) for several final rotational states j' is plotted (at $\beta = 180°$), as are some corresponding Legendre polynomials. The dashed line with label $\eta_{\max}$ indicates the position where the phase shift is maximum (least negative) and

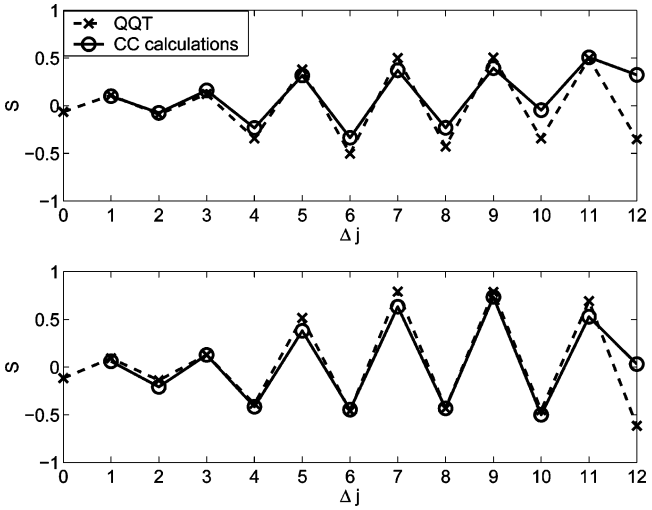

Figure 9. QQT results for the steric asymmetry ratio of He−NO collisions ($\Omega' = {}^1/_2$), compared to results of CC (HIBRIDON) calculations.[6] Mixing coefficients used are $\alpha(E) = 0.883$ and $\beta(E) = 0.470$,[6] and the collision energy is approximately 510 cm^{-1}. The upper panel denotes $\epsilon' = -1$, while the lower shows results for $\epsilon' = 1$. In the case of perfect orientation (mixing), both panels should show the same result, as both components of the Λ-doublet are equally populated before the collision.

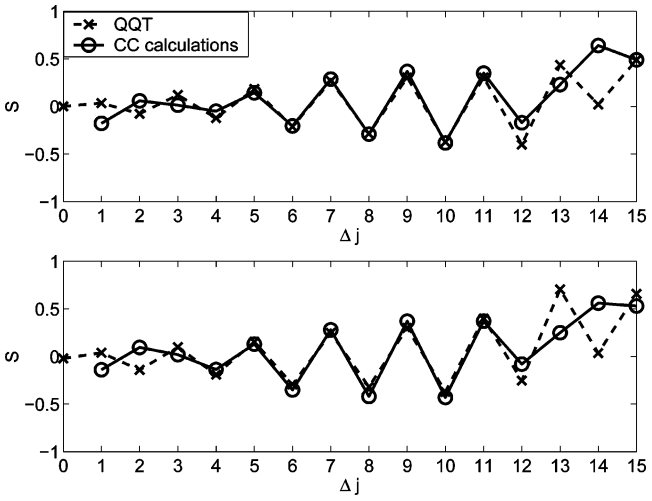

Figure 10. QQT results for the steric asymmetry ratio of Ar−NO collisions ($\Omega' = {}^1/_2$, $\epsilon' = 1$), compared to results of CC (HIBRIDON) calculations.[5,8] Mixing coefficients used are $\alpha(E) = 0.832$ and $\beta(E) = 0.555$,[4] and the collision energy is approximately 510 cm^{-1}. The upper panel denotes $\epsilon' = -1$, while the lower shows results for $\epsilon' = 1$. The differences between the QQT results and the CC results for $\Delta j \leq 3$ likely originate from attractive long-range interactions that are neglected in the hard-shell QQT calculations. Aoiz et al.[48] showed that the attractive part of the potential only has significant influence for $\Delta j \leq 3$.

stationary. This position dominates within the integral, which is enhanced by the fact that $g_{\text{class}}(\gamma_a;\beta)$ has a maximum at this position (the waist of the molecule) as well. Except at the stationary phase point, the molecule-fixed scattering amplitude will show oscillations around 0 where the phase is not stationary, which yields a small contribution in this area. On the other hand, if there is a too large area of stationary phase compared to the oscillations of the Legendre polynomials, the contribution in that area will also be close to 0. This is the reason that the cross section for excitation to high rotational states vanishes for glancing collisions with small phase shifts.

To illustrate how the stationary phase defines the sign of the steric asymmetry, scattering into $j' = 6.5$ is discussed here in some detail. Recall that, in the integral for the scattering amplitude, a sum of two integrals of Legendre polynomials is found (eq 28):

$$\frac{\mathrm{d}\sigma_{1/2,\pm\rightarrow j'}}{\mathrm{d}\omega} = \frac{j' + {}^1/_2}{4k^2} C(\beta)^2 \frac{\sin\beta}{\sin\vartheta}\left|\frac{\partial\beta}{\partial\vartheta}\right| \left|g_{j'-1/2}(\beta) \pm g_{j'+1/2}(\beta)\right|^2$$

with

$$g_n = \int_{-1}^{1} g_{\text{class}}(\gamma_a;\beta)\, \mathrm{e}^{i\eta(\gamma_a;\beta)} P_n(\cos\gamma_a)\, \mathrm{d}\cos(\gamma_a).$$

The "±" defines orientation, whereas the "+" indicates an R−NO collision and the "−" an R−ON collision. Recall that the apse serves as the quantization axis here. Scattering will be dominated by the value of the Legendre polynomial around the phase shift maximum $\gamma_{\max}$ (where $\eta(\gamma_a;\beta) = \eta_{\max}$). For now, a spherical hard shell is assumed, so $g_{\text{class}}(\gamma_a;\beta)$ is independent of γ_a. Roughly speaking, for $j' = 6.5$ one has

$$g_6 \sim \mathrm{e}^{i\eta_{\max}} P_6(\cos\gamma_{\max}) = -0.27\, \mathrm{e}^{i\eta_{\max}}$$

$$g_7 \sim \mathrm{e}^{i\eta_{\max}} P_7(\cos\gamma_{\max}) = 0.18\, \mathrm{e}^{i\eta_{\max}} \qquad (48)$$

For an N-end collision, $g_6 + g_7 = -0.09\, \mathrm{e}^{i\eta_{\max}}$ appears in the integral, while for an O-end collision one has $g_6 - g_7 = -0.45\, \mathrm{e}^{i\eta_{\max}}$. It is easily seen that the latter will yield a larger contribution to the differential cross section for a transition to $j' = 6.5$:

$$\frac{\mathrm{d}\sigma_{1/2,-\rightarrow j'=6.5}}{\mathrm{d}\omega} > \frac{\mathrm{d}\sigma_{1/2,+\rightarrow j'=6.5}}{\mathrm{d}\omega} \qquad (49)$$

According to eq 1, this will give a negative steric asymmetry, which is also seen in Figure 9. The steric asymmetry will be slightly weakened, as explained by eq 36. The values for S in Figures 9 and 10 are not calculated using the stationary phase argument, but the whole integral in eq 32 is evaluated.

Besides integral cross sections and thus steric asymmetries, the QQT provides differential cross sections. Although until now no differential cross sections have been measured for collisions of oriented NO, they are available for collisions of nonoriented NO with He. Westley et al.[49] performed ion imaging measurements using state selection of the NO with adiabatic cooling for state selection (both components of the Λ-doublet present). Recently, Gijsbertsen et al. performed ion imaging experiments with hexapole state-selected NO, in which only the upper component of the Λ-doublet ($\epsilon = -1$) is present.[13] Some (raw) ion images[13] are shown in Figure 4. The intensity on an outer ring of these images roughly indicates the differential cross section. In Figure 12, some differential cross sections from the QQT are compared to (extracted) experimental data and data from close-coupling calculations. The extraction method is explained in ref 13. The QQT results and experimental data are normalized to the integral cross sections available from HIBRIDON results to enable a good comparison of the angular dependence. There is a difference between the integral cross sections of the

(48) Aoiz, F. J.; Verdasco, J. E.; Herrero, V. J.; Sáez Rábanos, V.; Alexander, M. H. *J. Chem. Phys.* **2003**, *119*, 5860.
(49) Westley, M. S.; Lorenz, K. T.; Chandler, D. W.; Houston, P. L. *J. Chem. Phys.* **2001**, *2*, 473.

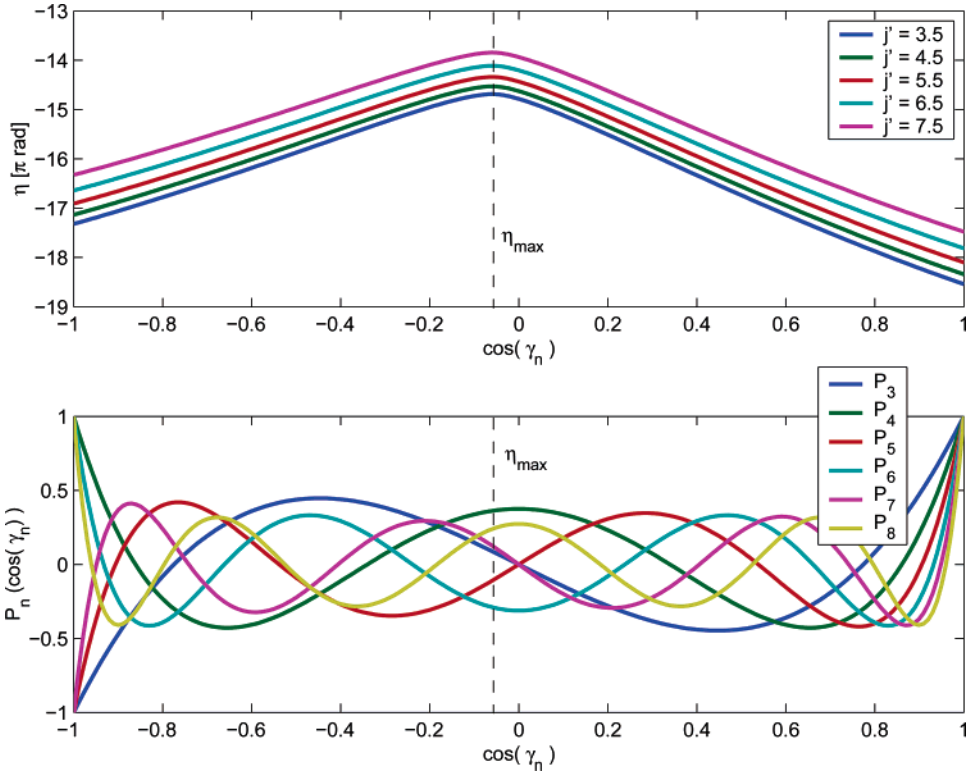

Figure 11. Combination of phase shift η (top panel) and the Legendre polynomials (lower panel) fix the sign of the steric asymmetry S. The phase shift drawn here is for collisions with $\beta = 180°$ (incoming momentum lies along the surface normal). The dashed line with label η_{max} indicates the position where the phase shift is maximum (least negative). At this point, the phase shift is stationary (the derivative $d\eta/d\gamma_a = 0$), which makes this position dominant within the integral, which is enhanced by the fact that $g_{class}(\gamma_a;\beta)$ has a maximum at this position. Due to the fact that k and k' are larger for Ar−NO than for He−NO, the phase function will be steeper for the Ar−NO system (see eq 42).

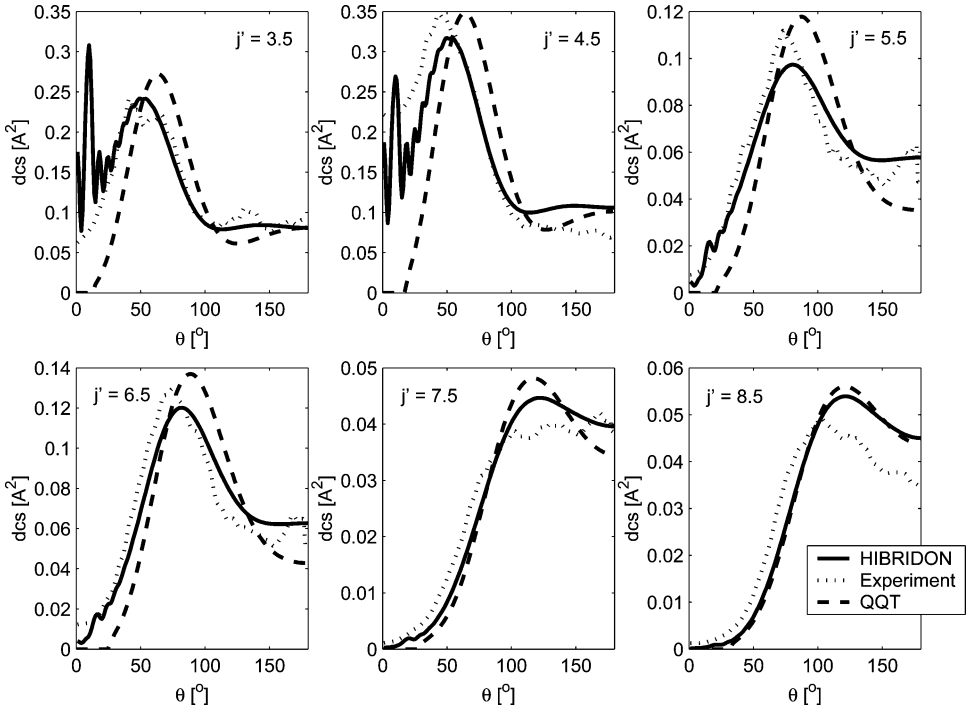

Figure 12. Several He−NO differential cross sections for parity-conserving transitions ($p = p' = -1$). The parity pairs (see also Figure 4) are easily seen in this figure. Both the experimental and QQT results are normalized on the integral cross section from close-coupling HIBRIDON results. The hard-shell approximation causes an underestimation of the differential cross section for low rotational states. For these differential cross sections, the normalization factors are (from low to high rotational states) 1.51, 1.58, 1.15, 1.18, 0.84, and 0.91.

HIBRIDON calculations and QQT calculations; normalization factors are provided in the caption of Figure 12. This is easily explained by the use of a hard shell. To transfer a lot of kinetic energy into rotation, the potential is more deeply penetrated, causing underestimation of the cross section for low rotational states. Scattering into $\bar{\Omega}' = {}^3/_2$ was not taken into account in

the QQT, which should result in too large a differential cross section overall for scattering into the $\bar{\Omega}' = {}^1/_2$ states.

5. Conclusions

The quasi-quantum-mechanical methodology successfully explains the steric asymmetry and its alternation based on interfering scattering trajectories from a single, purely repulsive potential energy surface. It is thereby demonstrated that the steric asymmetry reflects phase differences between scattering from the two ends of the NO molecule. This phase shift function defines the sign of the steric asymmetry, while the oscillation of $S_{i\rightarrow f}$ follows from the sum of − or difference between − the Legendre polynomials in the integral in eq 28. The straightforward quasi-quantum-mechanical picture provides the first physically simple, yet rigorous, explanation for the behavior of the steric asymmetry, and it can readily be extended to provide predictions of steric effects in other inelastic scattering systems or for reactive collisions. It is shown that the effect of the attractive part of the potential is small and thus that interference between propagation on the A' and A'' surfaces is not responsible for the oscillations.

The differential cross sections calculated for nonoriented NO molecules colliding with He atoms agree reasonably well with experimental results and coupled channel calculations. The QQT predicts a parity propensity rule that is also seen in experimental results and results from full quantum-mechanical calculations. This rule was not recognized as such until now. To improve the qualitative results of the QQT, the potential can be made softer. This will allow the potential to be penetrated more deeply in the case of head-on collisions than in the case of glancing collisions. Low rotational states will then show a larger cross section compared to the current results.

Acknowledgment. This work is part of the research program of the 'Stichting voor Fundamenteel Onderzoek der Materie (FOM), which is financially supported by the 'Nederlandse Organisatie voor Wetenschappelijk Onderzoek (NWO). The authors are very grateful to Dr. J. Bulthuis and Dr. D.W. Chandler for helpful discussions and thank M. Wisse and G. Boon for initial contributions. C.A.T. is supported by the Division of Chemical Sciences, Geosciences, and Biosciences, the Office of Basic Energy Sciences, the U.S. Department of Energy, and his participation was partially facilitated by a NATO collaborative travel grant. Sandia is a multiprogram laboratory operated by Sandia Corporation, a Lockheed Martin Company, for the U.S. Department of Energy's National Nuclear Security Administration under Contract DE-AC04-94-AL85000. S.S. thanks Prof. A. González Ureña for the warm hospitality and stimulating atmosphere during a sabbatical at the Instituto Pluridisciplinar.

Supporting Information Available: Complete ref 9 and a short discussion concerning the impact the QQT has on the discrepancy in the sign of the steric asymmetry ratio.[7,11] This material is available free of charge via the Internet at http://pubs.acs.org.

JA057828B